THE JOURNAL OF PHYSICAL CHEMISTRY B

Article

Cite This: J. Phys. Chem. B 2018, 122, 9538−9548

pubs.acs.org/JPCB

Dynamics and Microstructures of Nicotine/Water Binary Mixtures near the Lower Critical Solution Temperature

Heather E. Bailey, Yong-Lei Wang, Stephen R. Lynch, and Michael D. Fayer*

Department of Chemistry, Stanford University, Stanford, California 94305, United States

Supporting Information

ABSTRACT: The orientational dynamics and microscopic structures of nicotine/water binary mixtures near the system's lower critical solution temperature (LCST) were elucidated using optical heterodyne-detected optical Kerr effect (OHD-OKE) spectroscopy, nuclear magnetic resonance correlation spectroscopy (NMR COSY), first-principles calculations, and molecular dynamics simulations. Water concentrations were investigated from zero to close to pure water. At temperatures below the LCST, OHD-OKE experiments measured an anomalous slowing as the phase transition concentration was approached. At moderate concentrations and low temperatures, intermolecular cross-peaks between nicotine and water molecules were observed in the COSY spectra, demonstrating the formation of structures that persist for milliseconds. These results suggest that pair correlations contribute to the slowdown in the OHD-OKE data at moderate water concentrations. First-principles calculations revealed that intermolecular hydrogen bonding coordination between nitrogen atoms in pyridine moieties and water lowers the energy barriers for the reorientations of the two nicotine rings. Atomistic simulations demonstrate that with increasing water concentration, hydrogen bonding interactions between pyridine moieties and water molecules first increase and then decrease with a maximum at moderate water concentrations. These experimental and computational characterizations of the dynamics of nicotine molecules are attributed to the distinct configurations of water molecules around the pyridine ring moieties in nicotine molecules.

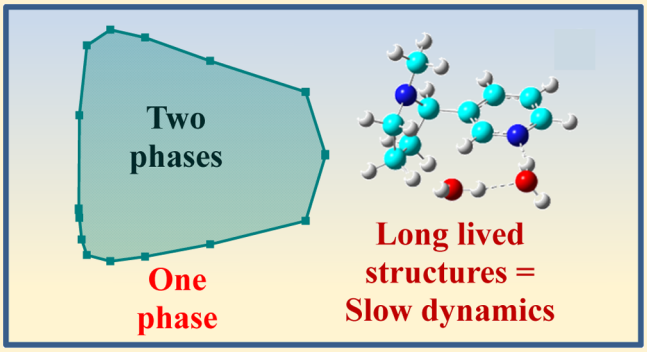

1. INTRODUCTION

Binary mixtures often exhibit anomalous phase behavior, particularly when the cosolvents are chemically dissimilar. One manifestation of this behavior is in the miscibility of two liquids. In the case of many binary mixtures, the miscibility of two liquids at a given concentration is highly temperature-dependent, with a two-phase region being observed at some temperatures and a one-phase, completely miscible region being observed at other temperatures in the same concentration sample. This temperature-dependent solubility has been of great interest because of its applications in varied fields including nanotechnology,[1] drug delivery,[2,3] and separations in organic synthesis.[4,5]

In binary mixtures that exhibit this behavior, the commonly observed phase transition occurs when the mixture becomes completely miscible as the temperature is increased above the upper critical solution temperature (UCST). UCSTs are ubiquitous in binary mixtures between dissimilar molecules and, consequently, the underlying physical phenomena are well understood in terms of the Gibbs free energy of mixing, given in eq 1[6]

$$\Delta G_{mix} = \Delta H_{mix} - T\Delta S_{mix} \quad (1)$$

where ΔH_{mix} is the enthalpy of mixing, T is the temperature, and ΔS_{mix} is the entropy of mixing. As temperature increases, the entropy term dominates. Thus, this high-temperature UCST transition is driven by favorable entropic contributions that overcome repulsive intermolecular interactions between dissimilar molecules.[7−9]

In some binary mixtures, there is an additional temperature-dependent phase transition that occurs as the temperature drops below the lower critical solution temperature (LCST). In these systems, the mixture becomes completely miscible again at low temperatures. When a system has both a UCST and an LCST, the resulting phase diagram is a closed solubility loop.[10] LCST behavior is relatively rare and generally happens when the dissimilar molecules can form strong hydrogen bonds.[8,10] Many recent studies on LCST behavior have focused on large, covalent polymers such as poly(*N*-isopropylacrylamide) because of their utility in nanotechnology and biology.[11−13] There are also studies on LCST behavior in ionic liquids with small-molecular-weight cosolvents such as water, acetone, and chloroform.[14−16] In addition, there have

Received: June 28, 2018
Revised: September 17, 2018
Published: September 19, 2018

DOI: 10.1021/acs.jpcb.8b06205
J. Phys. Chem. B 2018, 122, 9538−9548

been studies of small organic species with water,[17,18] some of which are particularly valuable systems because of their potential usage in chemical synthesis as extraction and separation processes could be completed simply by changing temperatures. The relative simplicity of these systems makes them ideal model systems for learning about the physical phenomena that underlie LCST behavior.

The first discovery of a closed solubility loop was the nicotine/water binary mixture by Hudson in 1904.[19] The structure of nicotine (−) is given in Figure 1. Note the

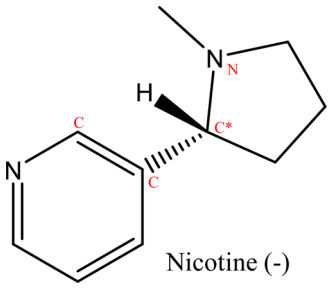

Figure 1. Chemical structure of nicotine. Note the presence of hydrogen bond acceptors (lone pairs on N) and lack of hydrogen bond donors. Definition of N−C*−C−C dihedral angle between two-ring planes in the nicotine molecule (red letters).

amphiphilic nature of nicotine, the presence of strong hydrogen bond acceptors (especially the lone electron pair of nitrogen atom in the pyridine moiety), and the lack of strong hydrogen bond donors.[20] The phase diagram for the nicotine/water system, adapted from the original Hudson paper, is given by the blue line in Figure 2 in terms of the mole fraction of

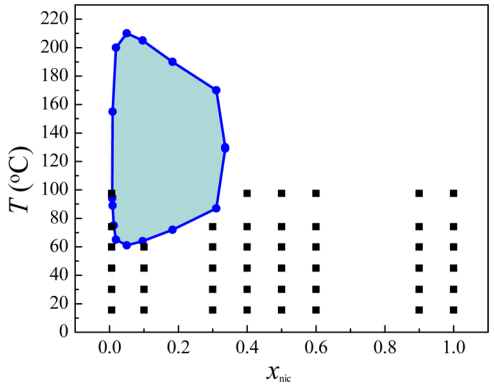

Figure 2. Phase diagram of nicotine/water binary mixtures as adapted from Hudson[19] (blue line). The shaded area inside the closed loop is the region in which nicotine and water are not infinitely miscible and phase-separate. The white area represents concentration/temperature ranges in which the liquids are infinitely miscible. The black squares show the temperatures and concentrations where OHD-OKE data were collected.

nicotine. In the shaded region enclosed by the solubility loop, the nicotine/water mixtures are immiscible and exist in two layers. Outside this loop, the nicotine/water mixtures are completely miscible. The LCST is at ∼60 °C and the UCST is at 208 °C.[19] The lower temperature region of this plot provides an opportunity to investigate the microstructures and dynamics associated with LCST transition.

In this work, we use optical heterodyne-detected optical Kerr effect (OHD-OKE) spectroscopy to measure the ultrafast orientational dynamics of nicotine molecules in binary mixtures of varying concentrations and temperatures with particular focus on the region near the LCST. OHD-OKE is an ideal technique for studying this system because it is nonresonant, so a probe molecule does not need to be added to obtain ultrafast data. As phase diagrams are very sensitive to impurities, this is a key advantage. The dynamical information obtained from OHD-OKE is complemented by two-dimensional nuclear magnetic resonance correlation spectroscopy (NMR COSY). Additional molecular simulations including first-principles calculations and subsequent atomistic simulations were performed to address the striking intermolecular interactions between different moieties in nicotine and water molecules. Previously, OHD-OKE and atomistic simulations have been used in conjunction to study phase behavior in binary mixtures of ionic liquids and water.[21,22] In the current work, these experimental and computational studies can provide extensive and valuable information on microstructures and dynamics that contribute to LCST-type behavior in nicotine/water mixtures.

2. EXPERIMENTAL AND COMPUTATIONAL PROCEDURES

2.1. Sample Preparation and Characterization. Nicotine was purchased from Sigma (>99% purity) and filtered using a 0.02 μm filter (Whatman Anotop) to remove scattering particles. The nicotine/water binary mixtures were prepared at multiple water concentrations by mass. The observed phase separation matched the temperature and concentration dependences reported in the literature.[19] The viscosity of each sample as a function of temperature was measured using a high-resolution rheometer (ARES-G2) with a water-cooled Advanced Peltier System to control the temperature. Viscosities were measured from 10 °C to the phase separation temperature (up to ∼100 °C for samples that do not separate). For the OHD-OKE experiments, all samples were transferred to a 1 cm optical grade cuvette. Sample temperature was controlled with a thermoelectric plate attached to a metal housing that made good thermal contact with the cuvette. The temperature was confirmed with a thermocouple in the liquid. The concentrations and temperatures at which OHD-OKE data were collected are shown by the black squares in Figure 2.

NMR data were collected on neat samples (i.e., no additional solvent) using a 600 MHz Varian INOVA NMR spectrometer equipped with a triple-resonance and z-gradient HCN probe at 25 °C. The ^{1}H one-dimensional spectrum was acquired unlocked with a 45° excitation pulse for four scans with an acquisition time of 5.8 s and a recycle delay of 1 s. NMR spectra were referenced indirectly to a sample of 1% tetramethylsilane in $CDCl_3$. Gradient-COSY data were acquired with two scans of 2048 points in t_2 by 200 points in t_1, with a spectral width of 5636 Hz in both dimensions for an acquisition time of 0.182 s and a recycle delay of 1.3 s.

2.2. OHD-OKE Spectroscopy. The OHD-OKE experiments were conducted at eight water concentrations at up to six temperatures. The OHD-OKE setup has been described previously,[23,24] but the key components are briefly described here. Ultrafast pulses are generated by an 86 MHz Ti:Sapphire oscillator and then amplified by a 5 kHz Ti:Sapphire regenerative amplifier. The amplified pulses are beam split into a pump beam and a probe beam. The pump beam is linearly polarized when it arrives at the sample. The probe beam arrives at the sample polarized at 45° relative to the

DOI: 10.1021/acs.jpcb.8b06205
J. Phys. Chem. B 2018, 122, 9538−9548

pump beam. It is variably delayed via a delay line for the collection of data at many time points. These points combine to give a complete orientational decay. Heterodyne detection is implemented using a Pockels cell to make the probe slightly elliptical prior to the sample. This results in a collinear local oscillator that couples with the signal and allows for phase cycling by switching the Pockels cell to change the handedness of the ellipticity.[25,26]

The OHD-OKE technique measures the time derivative of the polarizability−polarizability correlation function. Usually, after a very early time when collision-induced interactions can result in a collective (many molecules) contribution to the signal, the data are related to the second Legendre polynomial orientational correlation function $C_2(t)$. At the longest times of interest here, the decays are exponentials, and as the derivative of an exponential is the same exponential, the longtime data are $C_2(t)$. This method provides a way to track the motions of molecules from the picosecond range to the completion of their orientational dynamics many decades later. The experiment is a nonresonant pump-probe method in which the pump beam induces a birefringence. The delayed probe pulse measures the time dependence of the birefringence. As described by linear response theory, the liquid returns to its equilibrium state (and consequently the birefringence decreases) through equilibrium fluctuations of the liquid.

The orientational correlation function has been modeled using schematic mode coupling theory (MCT).[27] MCT uses a set of differential equations to couple the orientational correlation function (the integral of the OHD-OKE signal) with the density correlation function. These solutions give numerical decays for the two correlation functions, but they fail to provide an analytical description of the individual orientational randomization processes that give rise to the complete correlation functions. The MCT results generally can be described as one or more power laws followed by an exponential decay on the longest timescale.[28] To fit the data, a phenomenological fitting function, eq 2, based on the MCT results, is used.

$$F(t) = \frac{B}{2}\left(1 - \mathrm{erf}\left(\frac{(\ln(t) - n)}{\sqrt{2}u}\right)\right)t^{-b} + \frac{C}{2}\left(1 + \mathrm{erf}\left(\frac{\ln(t) - n}{\sqrt{2}u}\right)\right)e^{-t/\tau} + y_0 \quad (2)$$

Equation 2 has been described previously.[21] Because of the large number of parameters in eq 2, the final exponential is fit by itself using a single exponential. This is repeated over multiple time ranges where the value of τ is the same within the error of the fit. This ensures that the fits are completed in the purely exponential region. Using the exponential obtained in a long time, a global fit using eq 2 is performed to confirm the values of the exponential.

2.3. Simulation Methodology. The electronic structure calculations on both a single nicotine molecule and a nicotine/water complex were performed using the Gaussian 09 package (version D.01).[29] Molecular geometry optimizations were carried out at the B3LYP/6-311+G(d,p) level of theory. In the current work, density functional theory with the Grimme's-D3 dispersion correction[30] was used to obtain the optimized molecular structures of a single nicotine molecule and nicotine/water complexes. This dispersion correction is appropriate over medium (≈2−5 Å) and long ranges (>5 Å) and is an effective method to obtain binding structures of complexes with reduced computational cost. Multiple starting configurations of the nicotine molecule were optimized. Each of these was tested with harmonic frequency analysis, and all of the optimized configurations that were considered had no negative vibrational eigenvalues. Twenty starting configurations were tried. Of these, 18 relaxed to the same minimum. The two that did not relax to this minimum had higher conformational energy at their local minima. Therefore, the lowest energy minimum that was found from the multiple starting configurations was considered to be the global minimum. Additional first-principles calculations were performed at the same level of theory to obtain the N−C*−C−C (see Figures 1 and S1 in the Supporting Information) dihedral energy profiles to characterize the most probable distributions of the two-ring plane moieties in the single nicotine molecule and in the nicotine/water complex. In the geometry optimization of the single nicotine molecule, all degrees of freedom were allowed, except for the N−C*−C−C dihedral angle, which was varied in an angle step of 5°. This resulted in 72 optimized molecular conformations of nicotine with varied N−C*−C−C dihedral angles.

On the basis of these optimized molecular conformations, we introduced two water molecules at each nicotine conformation, and prepared 40 nicotine/water complexes with two water molecules randomly distributed around the nicotine molecule which has a specific N−C*−C−C dihedral angle. These 40 nicotine/water complexes are optimized at the B3LYP/6-311+G(d,p) level of theory with the inclusion of Grimme's-D3 dispersion correction. In the geometry optimizations, the N−C*−C−C dihedral angle in nicotine/water complexes was constrained during optimization. The other degrees of freedom, both within the nicotine molecule and among nicotine and water molecules, were allowed to move. For the 40 nicotine/water complexes with optimal conformations, we chose the one with the lowest conformational energy to be the optimized conformation for the nicotine/water complex with the specific N−C*−C−C dihedral angle to construct the potential energy surface.

Atomistic force field parameters for the nicotine molecule based on the Amber framework were developed in a similar procedure as that described in previous work.[21,22,31] The CHELPG atomic partial charges on the nicotine molecule were calculated at the same level of theory with the B3LYP hybrid functional and the 6-311+G(d,p) basis set. The SPC/E water model with constrained covalent bonds is employed in the current work. The crossinteraction parameters between different atom types are obtained from the Lorentz−Berthelot combination rules. In the subsequent atomistic simulations of nicotine/water binary mixtures, the number of nicotine and water molecules in each simulation system is determined to match the experimental nicotine/water mixture compositions. The detailed simulations system compositions for all binary nicotine/water mixtures with varied concentration ratios are provided in Table S3 in the Supporting Information.

Atomistic molecular dynamics simulations were performed using the GROMACS package[32] with three-dimensional periodic boundary conditions. The equations of motion were integrated using a leapfrog integration algorithm with a time step of 1.0 fs. A cutoff radius of 1.6 nm was set for short-range van der Waals interactions and real-space electrostatic interactions. The particle-mesh Ewald summation method with an interpolation order of 5 and Fourier grid spacing of

DOI: 10.1021/acs.jpcb.8b06205
J. Phys. Chem. B 2018, 122, 9538−9548

0.12 nm was employed to handle long-range electrostatic interactions in reciprocal space. All simulation systems were first energetically minimized using a steepest descent algorithm and annealed gradually from 800 to 373 K within 10 ns and thereafter equilibrated for 20 ns. For each nicotine/water binary mixture, ensembles at temperatures of 353, 333, 323, and 303 K were derived from this system and were annealed for 20 ns to the target temperatures. All annealed simulation systems were equilibrated in an isothermal−isobaric (NPT) ensemble for 40 ns maintained using the Nosé−Hoover thermostat and the Parrinello−Rahman barostat with time coupling constants of 500 and 200 fs, respectively, to control the temperature and pressure at 1 atm. Canonical ensemble simulations were further performed for 100 ns for all nicotine/water mixtures, and the simulation trajectories were recorded at an interval of 100 fs for structure and dynamics analysis.

3. RESULTS AND DISCUSSION

3.1. OHD-OKE Experimental Results. As discussed above, the OHD-OKE experiment measures the derivative of the polarizability−polarizability correlation function. Thus, any molecule with anisotropic polarizability will contribute to the signal. Water has very small anisotropic polarizability,[33−35] particularly compared to nicotine with its aromatic ring. Thus, in the data described below, the signal originates essentially from the nicotine molecules. However, if the nicotine reorients, neighboring species must reorient, so the OHD-OKE data involves the total liquid randomization.

OHD-OKE data were collected at eight water concentrations ranging from neat nicotine to almost all water (x_{nic} = 0.006). This range of concentrations permitted experimental data to be collected on both sides of the solubility loop and below the solubility loop. A temperature dependence was performed for each concentration ranging from 15.5 °C to the phase transition temperature (97.0 °C in nicotine/water samples that were miscible at all temperatures). The temperatures and concentrations studied using OHD-OKE are shown by the black squares in Figure 2. Representative OHD-OKE data are given in Figure 3A for x_{nic} = 0.9 and Figure 3B for x_{nic} = 0.4, respectively. These plots focus on the exponential region that is characterized by time constant τ from eq 2, which reflects the complete orientational relaxation of the systems. The inset of Figure 3B shows the complete data including the power law region for x_{nic} = 0.4 at T = 30.0 °C. Note the logarithmic axes in the inset. The red dashed line shows a representative fit using eq 2. All fits were of similar quality. The power law reflects the short time non-Markovian dynamics in which a molecule is "caged" by the surrounding molecules.

The longtime exponential region, characterized by τ in eq 2, is of particular interest as it provides information on the timescale of complete molecular reorientation of nicotine in varied mixtures. In both panels of Figure 3, it is clear that the dynamics speed up as temperature increases. This is true at all concentrations studied in the current work. The concentration dependence of τ in the nicotine/water mixtures is of particular interest. In many systems including ionic liquids[21,24] and simple molecular liquids,[36,37] the addition of water results in faster orientational dynamics as measured by OHD-OKE. In rare cases that are usually accompanied with a phase transition such as gelation,[23] the relationship between τ and water concentration can be more complicated.

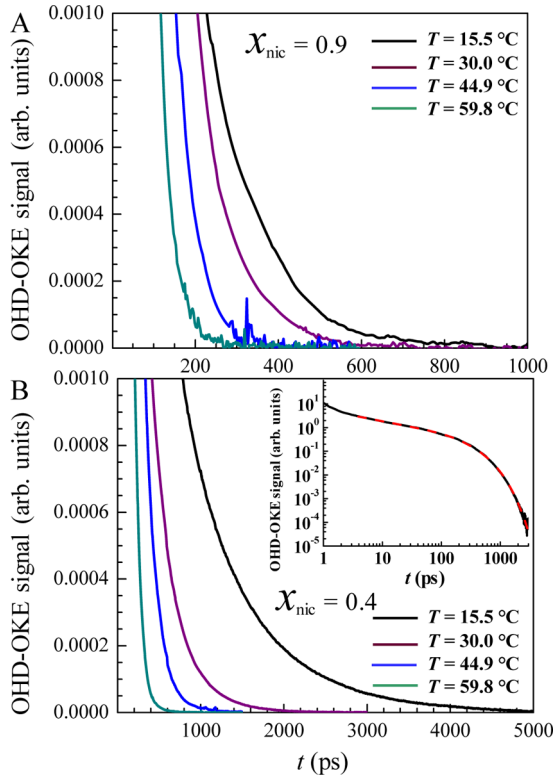

Figure 3. Representative temperature-dependent OHD-OKE data for nicotine/water mixtures at (A) x_{nic} = 0.9 and (B) x_{nic} = 0.4. The inset shows an entire curve including the short time power law portion on a log plot (black curve) and a fit (red dashed curve) using eq 2.

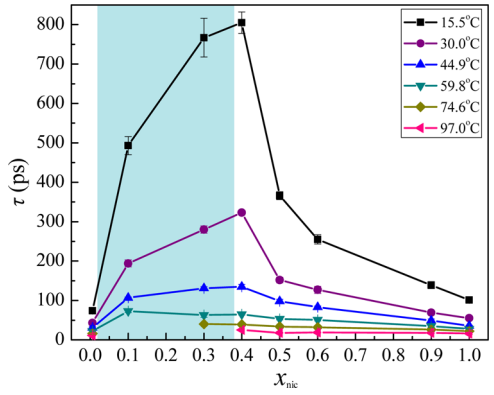

Figure 4. OHD-OKE measured time constants for six temperatures over a range of concentrations. Lines are included as aids to the eye. The blue region shows the concentrations where the solubility loop exists. The orientational dynamics slow significantly at low temperature as the phase separation concentration is approached.

The OHD-OKE time constants as a function of water concentrations at six temperatures are plotted in Figure 4. These τ values are listed in Table S1 in the Supporting Information. The blue-shaded region in Figure 4 represents the concentrations where the solubility loop exists. The lines are included as aids to the eye. As water is added to the bulk nicotine sample to form nicotine/water mixtures, initially the orientational dynamics of nicotine molecules slow down as the water concentration increases and approaches the solubility loop. At the highest temperature (T = 97.0 °C, pink), the slowdown is minimal, whereas the slowdown at the lowest temperature (T = 15.5 °C, black) is substantial. At all

DOI: 10.1021/acs.jpcb.8b06205
J. Phys. Chem. B 2018, 122, 9538−9548

temperatures, the orientational dynamics at x_{nic} = 0.4 are significantly slower than the dynamics of the neat liquids and mixtures.

The rate at which τ changes at different temperatures as the solubility loop concentration is approached is explored in Figure 5. The shaded region represents the temperatures where

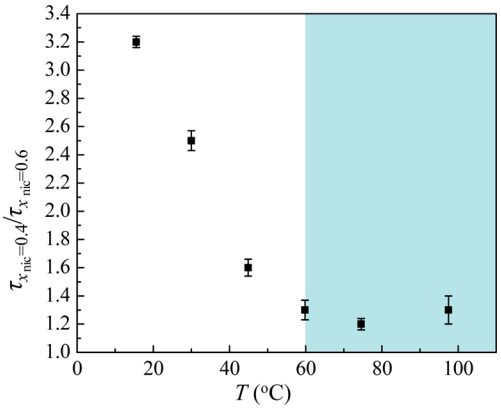

Figure 5. Ratios of τ values of x_{nic} = 0.4 and x_{nic} = 0.6 showing how rapidly the orientational dynamics change as the temperature is varied and the solubility loop concentration is approached.

the solubility loop exists. In this figure, the ratio between τ at x_{nic} = 0.4 and τ at x_{nic} = 0.6 is plotted as a function of temperature. The LCST for the nicotine/water binary system is ~60 °C. For the three temperatures at or above LCST, the ratio is the same within error. Below the LCST, the ratio steadily increases as the temperature decreases. The orientational dynamics of nicotine molecules are not constant across temperatures. The results imply that the microstructures in these nicotine/water mixtures involve significant interactions between nicotine and water molecules. The very substantial slowing of the dynamics of the 0.4 solution, which is at the edge of the low water concentration side of the solubility loop as the temperature is decreased (Figure 4) and the large change in the time constant ratio of the 0.4/0.6 solutions (Figure 5), indicates that changes in orientational dynamics and associated microstructures are related to the LCST and the miscibility at low temperatures.

As will be discussed below in detail, in the subsections on the NMR COSY experiments and the atomistic simulations, at moderate concentrations and low temperature distinct nicotine/water structures form. In these circumstances, the bulk dynamics measured in OHD-OKE experiments can deviate from single-molecule orientational relaxation, and the experiment reports on the relaxation of collective structures. Generally, such deviation from the measurement of single-molecule orientational relaxation only occurs at very short times. However, when collective interactions preserve some degree of the pump pulse-induced polarizability anisotropy for times longer than the single-molecule reorientation time, the experiment is sensitive to the relaxation of the collective polarizability anisotropy. At low and high water concentrations, nicotine/water structures do not exist to a significant extent, and the OHD-OKE experiment reports the single-molecule orientational relaxation.

In most liquids, orientational dynamics (and τ) speed up as temperature increases. This relationship is described by the generalized Debye−Stokes−Einstein (DSE) equation given in eq 3

$$\tau_{self} = \frac{\eta(T) V f_\theta C}{k_B T} \tag{3}$$

where τ_{self} is the single-molecule rotational self-diffusion time for a symmetric top, η is the temperature-dependent shear viscosity, V is the volume of the rotator, k_B is the Boltzmann constant, T is the absolute temperature, f_θ is a shape factor that accounts for friction because of the deviation of the rotator from sphericity,[38] and C is an interaction factor that accounts for friction because of the rotator dragging neighboring species as it reorients.[39] The OHD-OKE experiment measures the collective dynamics of a liquid which can differ from the single-molecule dynamics. To account for the possible role of collective dynamics, additional terms modify eq 3. The DSE equation as adapted for collective motion is given in eq 4

$$\tau = \frac{g_2}{j_2}\tau_{self} \tag{4}$$

where τ_{self} is the time constant from eq 2, g_2 is the static orientational correlation function, and j_2 is the dynamic orientational correlation function. j_2 has been determined to be near unity for many liquids.[40−42] g_2 describes the time-independent component of the orientational correlation function, which is mainly attributed to pair correlations, which will be present in structured liquids, for example, the nematic phase of liquid crystals. Thus, when comparing techniques that measure collective dynamics such as OHD-OKE to techniques that measure single-molecule dynamics, such as fluorescence depolarization anisotropy experiments, differences can be attributed to the presence of distinct pair correlations between ionic species. For many liquids, after a very short time the ratio of g_2/j_2 is unity, and the OHD-OKE experiment reports the single-molecular orientational relaxation time.

The DSE equation can be used to test a system for hydrodynamic behavior. Samples that exhibit hydrodynamic behavior will present as a linear feature when τ is plotted versus viscosity/temperature as all other parameters should remain unchanged. Nonlinear results indicate a nonhydrodynamic sample because of changes to structural parameters such as C and g_2. The DSE plots for nicotine/water mixtures are shown in Figure 6 for x_{nic} = 0.9 (A), x_{nic} = 0.4 (B), and x_{nic} = 0.006 (C). The liquid viscosities of these nicotine/water mixtures are provided in Table S2 in the Supporting Information. In panels (A,B), a solid line is included that is fit through the four highest temperature data points. This is extended and serves as an aid to the eye.

In the DSE plot in Figure 6A with x_{nic} = 0.9, the low-temperature data points deviate from the hydrodynamic line mildly. At the 15.5 °C data point, the largest deviation of 17% is observed. In the DSE plot in Figure 6B for the nicotine/water mixture with x_{nic} = 0.4, the two lowest data points deviate from the hydrodynamic line again. The deviation is larger at 45% at 15.5 °C. These DSE data are suggestive that there is a fundamental microstructural change as the temperature is reduced below the LCST. This is observed even at concentrations where the nicotine and water are infinitely miscible at all temperatures. However, this microstructural change is more pronounced at moderate water concentrations where the OHD-OKE dynamics slow down

DOI: 10.1021/acs.jpcb.8b06205
J. Phys. Chem. B 2018, 122, 9538−9548

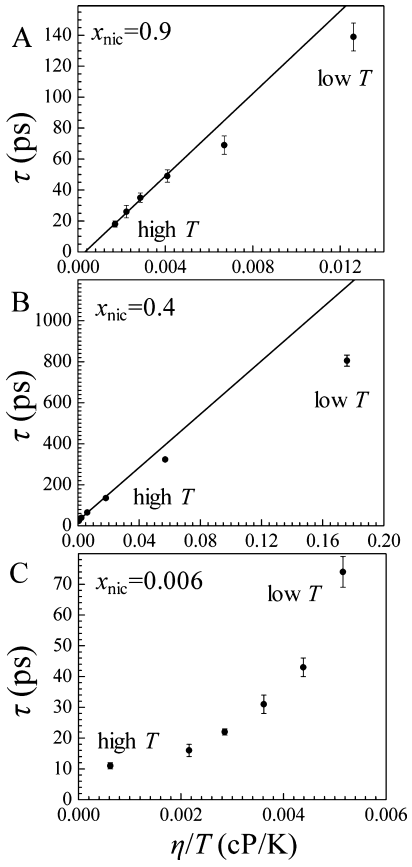

Figure 6. DSE plots for nicotine/water binary mixtures at representative concentrations. (A) x_{nic} = 0.9; (B) x_{nic} = 0.4; and (C) x_{nic} = 0.006. In panels (A,B), lines were fit through the four highest temperature data points and serve as an aid to the eye.

and the bulk viscosities increase greatly. These structures are based on the formation of strong, long-lasting hydrogen bonds between neighboring nicotine and water molecules, as will be discussed in Sections 3.2 and 3.3. It is worth noting that it is possible to fit all of the data points in Figure 6A,B with a line. However, as shown in Figure S5 in the Supporting Information, these fits result in residuals that display systematic deviations from the fit lines. The residuals indicate that a line through all of the data points is not the correct functional form. Furthermore, the deviations from linearity of the data shown in Figure 6 are consistent with the material presented in Sections 3.2 and 3.3.

Figure 6C gives the DSE plot for the nicotine/water mixture with x_{nic} = 0.006, which is on the low nicotine concentration side of the solubility loop. The DSE plot clearly has a different shape than that on the high nicotine concentration side of the solubility loop. This can be rationalized by the presence of different microstructures at low nicotine concentrations that underlie the infinitely miscibility at x_{nic} = 0.006. It is possible that the low nicotine concentration miscibility is due to water solvating individual nicotine molecules as opposed to strong, long-lasting hydrogen bonds between nicotine and neighboring water molecules.

3.2. First-Principles Calculations and Atomistic Simulations. The N−C*−C−C dihedral energy profiles between the two-ring plane moieties in nicotine are obtained from first-principles calculations. The N−C*−C−C dihedral energy profiles for a single nicotine molecule and for a nicotine/water complex, as well as the corresponding representative molecular structures, are shown in Figure 7. Both the single nicotine

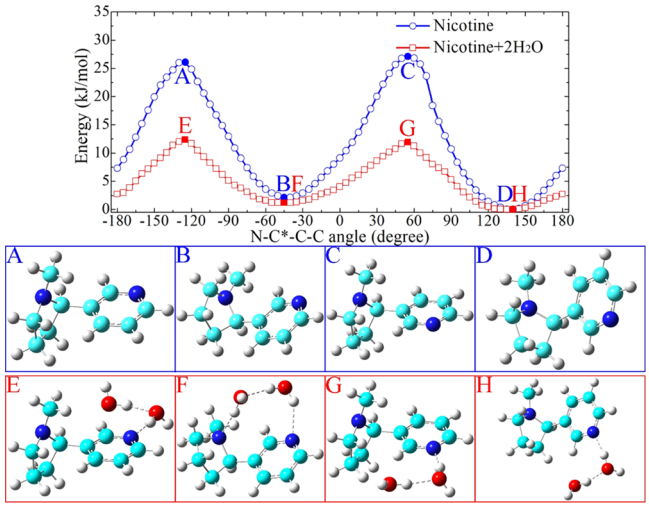

Figure 7. N−C*−C−C dihedral energy profiles for a single nicotine molecule and for a nicotine/water complex. Representative molecular structures are present for nicotine and nicotine/water complexes with the highest and lowest conformational energies.

molecule and the nicotine/water complex exhibit similar features with a 180° period. As described below, there are two minima that are less than kT different in energy. The two minima are at the N−C*−C−C angles of 140° and −45°. The corresponding maxima are at 55° and −130°, respectively. For the single nicotine molecule, the minima indicate that the two-ring moieties take preferential orientational distributions such that the intramolecular coordination is minimized. The energy profile of N−C*−C−C shows that there is a large energy barrier, ∼27 kJ/mol, separating the two minima. These quantum chemical calculation results are consistent with the results from similar quantum chemical calculations conducted by Pagliai et al.[43]

When water molecules are introduced, they have significant hydrogen bonding interactions with the pyridine moiety via the nitrogen atom,[43,44] which substantially decreases the energy barriers to ∼12 kJ/mol for the two-ring moieties to undergo reorientation. It is noteworthy that the strong hydrogen bonding interactions between water and nicotine do not change the N−C*−C−C angles found for the maxima and minima in the dihedral energy profiles. As can be seen in Figure 7, lowering the barriers by addition of water also broadens the angular range around the minima relative to thermal energy. For example, in the absence of water, the angular range around the −45° minimum that is within kT of the minimum is 47°. In contrast, with the addition of water, the angular range within kT around the same minimum is 76°. Thus, in the nicotine/water mixtures, more nicotine configurations are thermally accessible. The distinct intermolecular interactions between nicotine and water molecules and the formation of preferential nicotine/water complexes are likely to be important factors in the reorientational dynamics in nicotine/water mixtures.

Extensive atomistic molecular dynamic simulations were performed to address the distinct intermolecular interactions between nicotine and water molecules in mixtures with varied compositions at different temperatures. Figure 8 presents the

DOI: 10.1021/acs.jpcb.8b06205
J. Phys. Chem. B 2018, 122, 9538−9548

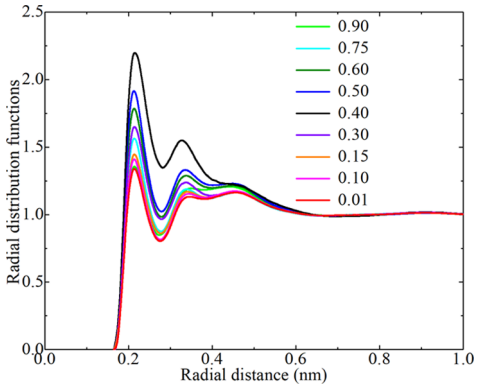

Figure 8. $N_{pyridine}$–H_{water} RDF plots in nicotine/water mixtures with various nicotine mole fractions (x_{nic}) at 333 K.

radial distribution functions (RDFs) between nitrogen atoms in pyridine moieties ($N_{pyridine}$) in nicotine and hydrogen atoms in water molecules (H_{water}) at 333 K. The RDFs between nitrogen atoms in pyrrolidino moieties ($N_{pyrrolidino}$) and H_{water} atoms exhibit similar features as those of $N_{pyridine}$–H_{water} RDFs and are provided in Figure S2 in the Supporting Information. The first peaks in the $N_{pyridine}$–H_{water} RDF plots indicate the formation of hydrogen bonds between pyridine moieties and water molecules.[43,44] However, such a hydrogen bonding feature is not available in the $N_{pyrrolidino}$–H_{water} RDFs because of distinct hydrophobic chemical environments around nitrogen atoms in pyrrolidino moieties.

With the addition of water, the first peak and the subsequent peaks in the $N_{pyridine}$–H_{water} and $N_{pyrrolidino}$–H_{water} RDFs increase in amplitude, indicating that the intermolecular interactions between pyridine moieties and water molecules, mediated by preferential hydrogen bonding coordinations, are getting stronger. These water molecules tend to locate around pyridine and pyrrolidino moieties of the same nicotine molecule, to mediate their relative orientations through distinctive hydrogen bonding interactions,[44] and to tune the distributions of pyridine moieties of neighboring nicotine molecules in nicotine/water/nicotine complexes. Such microstructures in nicotine/water mixtures are similar to those observed in ionic liquid/water mixtures,[21,22,45] but are different to those found in dimethyl sulfoxide/water mixtures.[46,47] The dimethyl sulfoxide/water mixtures' study demonstrated that even at very low water concentrations, water molecules prefer to form hydrogen bonds with other water molecules, leading to the formation of water clusters. It should be noted that the hydrophobic feature of the pyrrolidino ring moieties prevents water molecules from approaching the nitrogen atoms in pyrrolidino ring planes.[44]

The height of the first peak in the RDF plots for the nicotine/water mixture at x_{nic} = 0.4 is higher than those for the other mixtures. This corresponds to the formation of distinct nicotine/water interactions, which inhibits the reorientational motion of nicotine molecules in the mixture. The further addition of water molecules to the nicotine/water mixtures leads to decreased peak intensities in the $N_{pyridine}$–H_{water} and $N_{pyrrolidino}$–H_{water} RDFs. These computational results suggest that the nicotine/water complex structures seen in the mixture of x_{nic} = 0.4 are becoming less well established as more water molecules are involved in coordinating a central nicotine molecule. These nicotine/water complexes may lower the energy barriers for the reorientational motion of two-ring moieties in local environments, as suggested from the first-principles computational results shown in Figure 7. All of these observations are consistent with the reorientational dynamics of nicotine molecules in water mixtures as observed by the OHD-OKE experimental measurements shown in Figure 4.

The effects of temperature on the intermolecular interactions between pyridine/pyrrolidino moieties in nicotine molecules and water molecules, as characterized by $N_{pyridine}$–H_{water} and $N_{pyrrolidino}$–H_{water} RDFs, are provided in Figure S3 in the Supporting Information for four nicotine/water mixtures with x_{nic} = 0.9, 0.6, 0.4, and 0.15, respectively. For all four of these nicotine/water mixtures, the peak intensities for $N_{pyridine}$–H_{water} and $N_{pyrrolidino}$–H_{water} RDFs gradually decrease with an increase in temperature. This is attributed to the thermal motions of the molecules in mixtures, which tend to partially destabilize the nicotine/water complexes and thus lead to increased reorientational dynamics of nicotine molecules in binary mixtures.

The orientational dynamics of nicotine molecules in the various mixtures at different temperatures are represented by the second-rank Legendre polynomial correlation function.[22,48] The orientational correlation functions obtained from the atomistic simulations can be approximated by an exponential decay function. The orientational correlation times are then obtained by fitting the correlation functions. The simulated orientational correlation times for nicotine molecules in nicotine/water mixtures at 303, 333, and 373 K are shown in Figure 9 in comparison with those obtained from OHD-OKE experiments at similar temperatures.

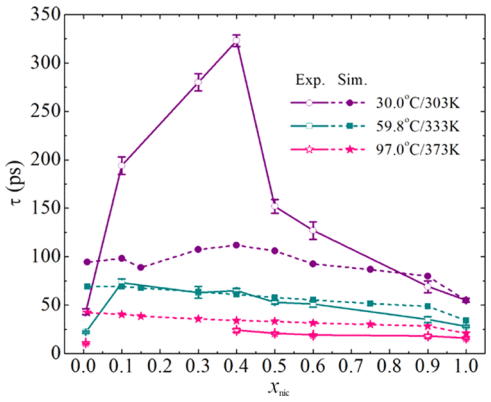

Figure 9. Comparison of orientational correlation times of nicotine molecules obtained from extensive molecular dynamic simulations with those measured with OHD-OKE experiments for various nicotine/water mixtures at different temperatures. The agreement between the simulations and measured values is very good except at the lowest temperature and for concentrations in and around the solubility loop (Figure 2).

For nicotine/water mixtures at high temperatures, such as at 333 and 373 K, and for nicotine/water mixtures at low water concentrations, the reorientational correlation times obtained from atomistic simulations are in very good agreement with those obtained from OHD-OKE experimental measurements. However, for nicotine/water mixtures with intermediate water concentrations, particularly x_{nic} = 0.4, significant discrepancy is observed between experimental and computational studies at low temperatures. The substantial differences at x_{nic} = 0.4 may be attributed to the formation of distinct molecular structures of the nicotine/water complexes. As discussed in connection

DOI: 10.1021/acs.jpcb.8b06205
J. Phys. Chem. B 2018, 122, 9538–9548

with eq 4, though the OHD-OKE experiment usually provides the single-molecule orientational relaxation time, it actually measures the decay of the anisotropic polarizability induced by the pump pulse. This induced anisotropy can relax more slowly than the single-molecule orientational relaxation time. The atomistic simulations calculate the single-molecule orientational relaxation. The good agreement between experiment and simulation shows that at most water concentrations and temperatures, the OHD-OKE experiment is measuring single-molecule (nicotine) orientational randomization. However, with long-lived multimolecule molecular complexes (see below), the collective polarizability anisotropy relaxation is slow compared to the single-molecular reorientation time, giving rise to the differences between the simulations and the experimental data. The value of g_2 in eq 4 deviates significantly from unity for concentrations and temperatures where the nicotine/water complexes exist. These nicotine/water complexes occur at low temperatures and concentrations near and in the solubility loop concentration range (see Figure 2).

3.3. NMR Spectroscopy. Additional structural information can be obtained from NMR measurements, particularly two-dimensional NMR COSY. COSY spectra were collected for nicotine/water mixtures at multiple concentrations at 25 °C to investigate the microstructures associated with the anomalous reorientational dynamics observed in OHD-OKE experiments at low temperatures and moderate concentrations (Figure 4, black and purple traces). The ^{1}H NMR spectrum of neat nicotine is shown in Figure 10 with peaks assigned to the protons in nicotine.

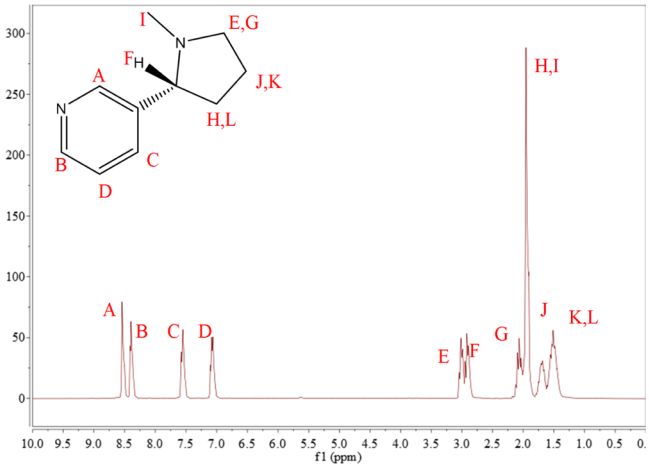

Figure 10. ^{1}H NMR spectrum of neat nicotine with peaks assigned to the hydrogens on the nicotine molecule.

Representative COSY spectra are shown in Figure 11 for x_{nic} = 0.9 (panel A) and x_{nic} = 0.4 (panel B). Additional COSY spectra are shown in Figure S4 in the Supporting Information. The ^{1}H spectrum for the nicotine/water mixture with x_{nic} = 0.9 has a peak associated with the water protons at 4.26 ppm. Inspection of the COSY spectrum in Figure 11A indicates that there are no cross-peaks involving the water protons, suggesting no significant, long-lasting interactions between water and nicotine. As shown in Figure S4 in the Supporting Information, the COSY spectrum for the nicotine/water mixture with x_{nic} = 0.8 also shows no water-associated cross-peaks. This is in contrast to the COSY spectrum for x_{nic} = 0.4, the sample that had the slowest OHD-OKE dynamics. As

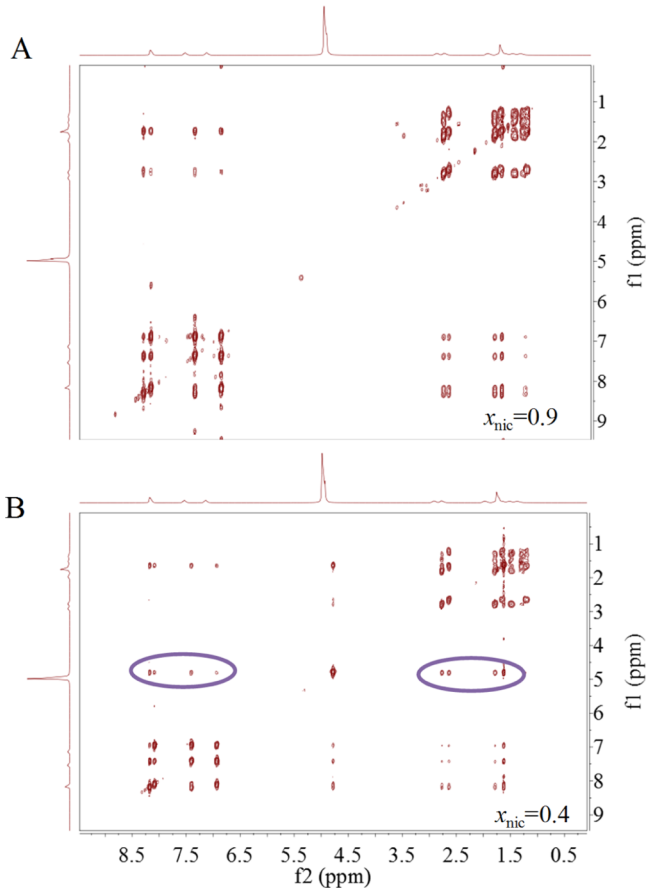

Figure 11. NMR COSY spectra of nicotine/water binary mixtures at x_{nic} = 0.9 (A) and x_{nic} = 0.4 (B). The ovals in (B) indicate the important off-diagonal peaks.

shown in Figure 11B, there are many cross-peaks between water and nicotine, with the strongest cross-peaks being associated with the hydrogen atoms closest to the nitrogen atoms of nicotine. The simulation results suggested that water favored pyridine interactions with the NMR data, confirming those interactions. The COSY spectra for x_{nic} = 0.6 and x_{nic} = 0.1 also have the same intermolecular cross-peaks. These intermolecular cross-peaks are an indicative of strong hydrogen bonds creating long-lasting structures that must persist into the millisecond regime to be observed with this technique. These cross-peaks (and the long-lasting microstructures) are not observed in nicotine/water mixtures with low water concentrations. It is important to note that water does not have cross-peaks with all protons of the nicotine molecules. Cross-peaks exist between the water protons A, B, C, E, F, G, and I (as labeled in Figure 10). This provides additional information on where water is located in these long-lasting structures.

Observing intermolecular water COSY cross-peaks is relatively rare, particularly at room temperature, because water usually exchanges rapidly. These cross-peaks are most commonly observed in samples that have been cooled to liquid nitrogen temperatures. However, they have also been observed at room temperature in biological samples such as proteins.[49,50] The limited number of samples where intermolecular water cross-peaks exist gives an indication of the uniqueness of the structural features observed here.

The COSY structural data can be related to OHD-OKE dynamics discussed in Section 3.1. The COSY spectra were

DOI: 10.1021/acs.jpcb.8b06205
J. Phys. Chem. B 2018, 122, 9538−9548

collected at a temperature between the two lowest OHD-OKE temperatures where the dramatic dynamical slowdown was observed. By comparing which concentrations have COSY intermolecular cross-peaks to the slowdown observed in Figures 4 and 5, it is clear that these long-lasting hydrogen bond structures are associated with the slow dynamics in nicotine/water mixtures with moderate water concentration and low temperature. At low water concentrations, where there are no COSY cross-peaks, it can be reasonably assumed that the bulk dynamics are the single-molecule dynamics, and there are no multinicotine complex contributions to the signal. This can be verified by the close agreement of the orientational correlation times obtained from the OHD-OKE experiments and the atomistic simulations. This is clearly not the case for nicotine/water mixtures with moderate concentrations. Besides the atomistic simulation data presented in Figures 7 and S2 and S3 in the Supporting Information, the COSY data for the nicotine/water mixture with x_{nic} = 0.4 provide additional evidence for long-lasting and strong intermolecular structures persisting into the millisecond domain. This timescale is much longer than the dynamics probed in OHD-OKE experiments. Thus, OHD-OKE cannot be measuring single-molecule dynamics with a single nicotine molecule as the rotator. The experimental data from OHD-OKE experiments should be the multiparticle collective dynamics. On the basis of the long-lasting microstructures observed in the NMR COSY data and the distinct peak intensities in $N_{pyridine}-H_{water}$ RDFs in Figure 8, g_2 in eq 4 must deviate significantly from eq 1.

The NMR results demonstrate the existence of long-lasting microstructures and strong hydrogen bond networks at low temperature (below the LCST) and for mole fractions in the range and approaching the range where phase separation occurs at a higher temperature. The OHD-OKE data (Figure 4) show anomalously slow dynamics for mole fractions near and in the range of the phase separation concentrations and temperatures below the LCST. The simulated single-molecule orientational relaxation (Figure 9) agrees well with the OHD-OKE data at high temperatures (above the LCST) but not for temperatures below the LCST and mole fractions near and in the range of the phase separation. The single-molecule simulation comparisons to the OHD-OKE data that display a lack of agreement are consistent with the NMR results that show the OHD-OKE data do not arise from single nicotine molecule dynamics. However, at temperatures above the LCST and near the phase separation mole fractions, the OHD-OKE results do not display anomalously slow dynamics and are consistent with the single-molecule simulations. These results indicate that at higher temperatures, above the LCST, hydrogen bonding no longer gives rise to long-lasting microstructures, and the loss of the strong hydrogen bond networks as the temperature is increased may be the key factor for the existence of an LCST.

4. CONCLUDING REMARKS

The orientational dynamics and microstructures underlying the LCST-type behavior exhibited by the nicotine/water binary mixtures were investigated by OHD-OKE and NMR COSY spectroscopy, and by first-principles calculations and atomistic molecular dynamics simulations. The OHD-OKE measurements showed that the orientational dynamics slowed as the phase transition concentration was approached. This became more pronounced as the temperature was decreased below the LCST. The DSE plots took different shapes based on the water concentration in nicotine/water mixtures. Nicotine-rich concentrations deviated from linearity at low temperatures. This deviation became more significant as the phase transition concentration was approached.

The first-principles calculations demonstrated that the addition of water molecules to the bulk nicotine sample could significantly decrease the energy barriers for the reorientation of pyridine and pyrrolidino ring moieties because of the preferential hydrogen bonding interactions between nitrogen atoms in pyridine moieties and hydrogen atoms in water molecules. This is clearly observed in the $N_{pyridine}-H_{water}$ RDF plots obtained from extensive atomistic molecular dynamics simulations. With a gradual increase in water concentration in nicotine/water mixtures, the $N_{pyridine}-H_{water}$ hydrogen bonding interactions get stronger and achieve their maximum in the nicotine/water mixture with x_{nic} = 0.4. This is attributed to the distinct distribution of water molecules around pyridine ring moieties of nicotine molecules. The further addition of water molecules to nicotine/water mixtures leads to decreased peak intensities in the $N_{pyridine}-H_{water}$ RDF plots as these water molecules tend to modify the local relative distribution of nicotine molecules. These microstructural changes in nicotine/water mixtures are manifested in the orientational dynamics of nicotine molecules.

Finally, NMR COSY spectra of nicotine/water mixtures at moderate concentrations and low temperature (25 °C) showed intermolecular cross-peaks between water protons and particular protons of nicotine. This relatively rare phenomenon suggests the formation of long-lasting microstructures between nicotine and water molecules because of strong specific hydrogen bonding interactions.

■ ASSOCIATED CONTENT

Supporting Information

The Supporting Information is available free of charge on the ACS Publications website at DOI: 10.1021/acs.jpcb.8b06205.

OHD-OKE time constants; bulk viscosities of nicotine/water binary mixtures at various temperatures; first-principles calculations and atomistic simulations; additional COSY spectra; and linear fits and residuals for Figure 6A,B (PDF)

■ AUTHOR INFORMATION

Corresponding Author

*E-mail: fayer@stanford.edu. Phone: 650 723-4446.

ORCID

Yong-Lei Wang: 0000-0003-3393-7257

Michael D. Fayer: 0000-0002-0021-1815

Notes

The authors declare no competing financial interest.

■ ACKNOWLEDGMENTS

We thank Joseph E. Thomaz for helpful discussions. H.E.B. and M.D.F. acknowledge financial support from the Division of Chemistry, Directorate of Mathematical and Physical Sciences, National Science Foundation (NSF) (CHE-1461477). Y.-L.W. gratefully acknowledges the financial support from the Knut and Alice Wallenberg Foundation (KAW 2015.0417). Atomistic molecular dynamics simulations were performed using computational resources provided by Stanford University. The viscosity measurements were performed at the Stanford Nano

DOI: 10.1021/acs.jpcb.8b06205
J. Phys. Chem. B 2018, 122, 9538−9548

Shared Facilities (SNSF), supported by the National Science Foundation under award ECCS-1542152. NMR spectra were collected at the Stanford University Department of Chemistry NMR facility.

REFERENCES

(1) Ramanan, V. V.; Hribar, K. C.; Katz, J. S.; Burdick, J. A. Nanofiber-nanorod composites exhibiting light-induced reversible lower critical solution temperature transitions. *Nanotechnology* **2011**, *22*, 494009.
(2) Hoffman, A. S. Applications of thermally reversible polymers and hydrogels in therapeutics and diagnostics. *J. Controlled Release* **1987**, *6*, 297−305.
(3) Okano, T.; Bae, Y. H.; Jacobs, H.; Kim, S. W. Thermally on-off switching polymers for drug permeation and release. *J. Controlled Release* **1990**, *11*, 255−265.
(4) Freitas, R. F. S.; Cussler, E. L. Temperature sensitive gels as extraction solvents. *Chem. Eng. Sci.* **1987**, *42*, 97−103.
(5) Depuydt, D.; Liu, L.; Glorieux, C.; Dehaen, W.; Binnemans, K. Homogeneous liquid-liquid extraction of metal ions with non-fluorinated bis(2-ethylhexyl)phosphate ionic liquids having a lower critical solution temperature in combination with water. *Chem. Commun.* **2015**, *51*, 14183−14186.
(6) Hirschfelder, J.; Stevenson, D.; Eyring, H. A theory of liquid structure. *J. Chem. Phys.* **1937**, *5*, 896−912.
(7) Jackson, G. Theory of closed-loop liquid-liquid immiscibility in mixtures of molecules with directional attractive forces. *Mol. Phys.* **1991**, *72*, 1365−1385.
(8) Walker, J. S.; Vause, C. A. Reappearing phases. *Sci. Am.* **1987**, *256*, 98−105.
(9) Vause, C. A.; Walker, J. S. Effects of orientational degrees of freedom in closed-loop solubility phase diagrams. *Phys. Lett. A* **1982**, *90*, 419−424.
(10) Wang, J.; Anisimov, M. A.; Sengers, J. V. Closed solubility loops in liquid mixtures. *Z. Phys. Chem.* **2005**, *219*, 1273−1297.
(11) Schild, H. G. Poly(N-isopropylacrylamide): experiment, theory and application. *Prog. Polym. Sci.* **1992**, *17*, 163−249.
(12) Albertsson, P.-Å. Partition of cell particles and macromolecules in polymer two-phase systems. In *Advances in Protein Chemistry*; Elsevier: The Netherlands, 1970; Vol. *24*, pp 309−341.
(13) Wang, Y.-L.; Lawrence, R. S.; Lu, Z.-Y.; Laaksonen, A. Molecular dynamics study of aqueous solution of polyethylene oxide: Critical test of force field models. *Soft Mater.* **2013**, *11*, 371−383.
(14) Dong, S.; Heyda, J.; Yuan, J.; Schalley, C. A. Lower critical solution temperature (LCST) phase behaviour of an ionic liquid and its control by supramolecular host-guest interactions. *Chem. Commun.* **2016**, *52*, 7970−7973.
(15) Lachwa, J.; Szydlowski, J.; Najdanovic-Visak, V.; Rebelo, L. P. N.; Seddon, K. R.; da Ponte, M. N.; Esperança, J. M. S. S.; Guedes, H. J. R. Evidence for lower critical solution behavior in ionic liquid solutions. *J. Am. Chem. Soc.* **2005**, *127*, 6542−6543.
(16) Wang, Y.-L.; Sarman, S.; Kloo, L.; Antzutkin, O. N.; Glavatskih, S.; Laaksonen, A. Solvation structures of water in trihexyltetradecyl-phosphonium-orthoborate ionic liquids. *J. Chem. Phys.* **2016**, *145*, 064507.
(17) Davies, N. S.; Gillard, R. D. The solubility loop of nicotine: water. *Transition Met. Chem.* **2000**, *25*, 628−629.
(18) Balasubramanian, D.; Mitra, P. Critical solution temperatures of liquid mixtures and the hydrophobic effect. *J. Phys. Chem.* **1979**, *83*, 2724−2727.
(19) Hudson, C. The reciprocative solubility of nicotine in water. *Z. Phys. Chem.* **1904**, *47*, 113−115.
(20) Banyasz, J. L. The physical chemistry of nicotine. *Analytical Determination of Nicotine and Related Compounds and Their Metabolites*; Elsevier Science: The Netherlands, 1999; pp 149−190.
(21) Bailey, H. E.; Wang, Y.-L.; Fayer, M. D. Impact of hydrogen bonding on the dynamics and structure of protic ionic liquid/water binary mixtures. *J. Phys. Chem. B* **2017**, *121*, 8564−8576.
(22) Bailey, H. E.; Wang, Y.-L.; Fayer, M. D. The influence of hydrophilicity on the orientational dynamics and structures of imidazolium-based ionic liquid/water binary mixtures. *J. Chem. Phys.* **2018**, *149*, 044501.
(23) Sturlaugson, A. L.; Arima, A. Y.; Bailey, H. E.; Fayer, M. D. Orientational dynamics in a lyotropic room temperature ionic liquid. *J. Phys. Chem. B* **2013**, *117*, 14775−14784.
(24) Sturlaugson, A. L.; Fruchey, K. S.; Fayer, M. D. Orientational Dynamics of Room Temperature Ionic Liquid/Water Mixtures: Water-Induced Structure. *J. Phys. Chem. B* **2012**, *116*, 1777−1787.
(25) Kinoshita, S.; Sakai, Y.; Miyazaki, J.; Watanabe, J. Fundamental aspects of light scattering and optical kerr effect spectroscopy. *Eur. Phys. J.: Spec. Top.* **2012**, *209*, 1−100.
(26) Smith, N. A.; Meech, S. R. Optically-heterodyne-detected optical Kerr effect (OHD-OKE): applications in condensed phase dynamics. *Int. Rev. Phys. Chem.* **2002**, *21*, 75−100.
(27) Li, J.; Cang, H.; Andersen, H. C.; Fayer, M. D. A mode coupling theory description of the short- and long-time dynamics of nematogens in the isotropic phase. *J. Chem. Phys.* **2006**, *124*, 014902.
(28) Götze, W.; Sjögren, L. The mode coupling theory of structural relaxations. *Transp. Theory Stat. Phys.* **1995**, *24*, 801−853.
(29) Frisch, M. J.; Tucks, G. W.; Schlegel, H. B.; Scuseria, G. E.; Robb, M. A.; Cheesema, J. R.; Scalmani, G. V.; Barone, B.; Mennucci, G. A.; Petersson, H.; et al. *Gaussian 09*, Revision D.01; Gaussian, Inc.: Wallingford CT, 2009.
(30) Grimme, S.; Antony, J.; Ehrlich, S.; Krieg, H. A consistent and accurate ab initio parametrization of density functional dispersion correction (DFT-D) for the 94 elements H-Pu. *J. Chem. Phys.* **2010**, *132*, 154104.
(31) Wang, Y.-L.; Shah, F. U.; Glavatskih, S.; Antzutkin, O. N.; Laaksonen, A. Atomistic insight into orthoborate-based ionic liquids: force field development and evaluation. *J. Phys. Chem. B* **2014**, *118*, 8711−8723.
(32) Abraham, M. J.; Murtola, T.; Schulz, R.; Páll, S.; Smith, J. C.; Hess, B.; Lindahl, E. GROMACS: High performance molecular simulations through multi-level parallelism from laptops to supercomputers. *SoftwareX* **2015**, *1-2*, 19−25.
(33) Palese, S.; Schilling, L.; Miller, R. J. D.; Staver, P. R.; Lotshaw, W. T. Femtosecond optical Kerr effect studies of water. *J. Phys. Chem.* **1994**, *98*, 6308−6316.
(34) Taschin, A.; Bartolini, P.; Eramo, R.; Righini, R.; Torre, R. Optical Kerr effect of liquid and supercooled water: The experimental and data analysis perspective. *J. Chem. Phys.* **2014**, *141*, 084507.
(35) Torre, R.; Bartolini, P.; Righini, R. Structural relaxation in supercooled water by time-resolved spectroscopy. *Nature* **2004**, *428*, 296−299.
(36) Idrissi, A.; Bartolini, P.; Ricci, M.; Righini, R. Time resolved optical Kerr effect analysis of urea-water system. *J. Chem. Phys.* **2001**, *114*, 6774−6780.
(37) Chang, Y. J.; Castner, E. W., Jr. Femtosecond dynamics of hydrogen-bonding solvents. Formamide and N-methylformamide in acetonitrile, DMF, and water. *J. Chem. Phys.* **1993**, *99*, 113−125.
(38) Perrin, F. Mouvement brownien d'un ellipsoide - I. Dispersion diélectrique pour des molécules ellipsoidales. *J. Phys. Radium* **1934**, *5*, 497−511.
(39) Dote, J. L.; Kivelson, D.; Schwartz, R. N. A molecular quasi-hydrodynamic free-space model for molecular rotational relaxation in liquids. *J. Phys. Chem.* **1981**, *85*, 2169−2180.
(40) Allison, S. A. Low Reynolds number transport properties of axisymmetric particles employing stick and slip boundary conditions. *Macromolecules* **1999**, *32*, 5304−5312.
(41) Hu, C.-M.; Zwanzig, R. Rotational friction coefficients for spheroids with the slipping boundary condition. *J. Chem. Phys.* **1974**, *60*, 4354−4357.
(42) Tirado, M. M.; de la Torre, J. G. Rotational dynamics of rigid, symmetric top macromolecules. Application to circular cylinders. *J. Chem. Phys.* **1980**, *73*, 1986−1993.
(43) Pagliai, M.; Mancini, G.; Carnimeo, I.; De Mitri, N.; Barone, V. Electronic absorption spectra of pyridine and nicotine in aqueous

DOI: 10.1021/acs.jpcb.8b06205
J. Phys. Chem. B 2018, 122, 9538−9548

solution with a combined molecular dynamics and polarizable QM/MM approach. *J. Comput. Chem.* **2017**, *38*, 319−335.
(44) Egidi, F.; Russo, R.; Carnimeo, I.; D'Urso, A.; Mancini, G.; Cappelli, C. The electronic circular dichroism of nicotine in aqueous solution: a test case for continuum and mixed explicit-continuum solvation approaches. *J. Phys. Chem. A* **2015**, *119*, 5396−5404.
(45) Wang, Y.-L.; Sarman, S.; Glavatskih, S.; Antzutkin, O. N.; Rutland, M. W.; Laaksonen, A. Atomistic Insight into Tetraalkylphosphonium-Bis(oxalato)borate Ionic Liquid/Water Mixtures. I. Local Microscopic Structure. *J. Phys. Chem. B* **2015**, *119*, 5251−5264.
(46) Wong, D. B.; Sokolowsky, K. P.; El-Barghouthi, M. I.; Fenn, E. E.; Giammanco, C. H.; Sturlaugson, A. L.; Fayer, M. D. Water dynamics in water/DMSO binary mixtures. *J. Phys. Chem. B* **2012**, *116*, 5479−5490.
(47) Vishnyakov, A.; Lyubartsev, A. P.; Laaksonen, A. Molecular Dynamics Simulations of Dimethyl Sulfoxide and Dimethyl Sulfoxide−Water Mixture. *J. Phys. Chem. A* **2001**, *105*, 1702−1710.
(48) Wang, Y.-L. Competitive Microstructures Versus Cooperative Dynamics of Hydrogen Bonding and π-Type Stacking Interactions in Imidazolium Bis(oxalato)borate Ionic Liquids. *J. Phys. Chem. B* **2018**, *122*, 6570−6585.
(49) Warren, W.; Richter, W.; Andreotti, A.; Farmer, B. Generation of impossible cross-peaks between bulk water and biomolecules in solution NMR. *Science* **1993**, *262*, 2005−2009.
(50) Eriksson, M.; Leijon, M.; Hiort, C.; Norden, B.; Graeslund, A. Binding of .DELTA.- and .LAMBDA.-[Ru(phen)3]2+ to [d-(CGCGATCGCG)]2 Studied by NMR. *Biochemistry* **1994**, *33*, 5031−5040.

DOI: 10.1021/acs.jpcb.8b06205
J. Phys. Chem. B 2018, 122, 9538−9548